Available online at www.sciencedirect.com
ScienceDirect
Catalysis Today 123 (2007) 257–264
CATALYSIS TODAY
www.elsevier.com/locate/cattod

Carbon formation and its influence on ethanol steam reforming over Ni/Al_2O_3 catalysts

Andre L. Alberton [a], Mariana M.V.M. Souza [b], Martin Schmal [a,*]

[a] *Coppe/Peq/Nucat, Federal University of Rio de Janeiro, Brazil*
[b] *Escola de Quimica, UFRJ, Brazil*

Available online 2 April 2007

Abstract

Ethanol steam reforming was studied over Ni/Al_2O_3 catalysts. The effect of support (α- and γ-Al_2O_3), metal loading and a comparison between conventional H_2 reduction with an activation method employing a CH_4/O_2 mixture was investigated. The properties of catalysts were studied by N_2 physisorption, X-ray diffraction (XRD) and temperature programmed reduction (TPR). After activity tests, the catalysts were analyzed by scanning electron microscopy (SEM) and thermogravimetric analysis (TG/DTA). Ni supported on γ-Al_2O_3 was more active for H_2 production than the catalyst supported on α-Al_2O_3. Metal loading did not affect the catalytic performance. The alternative activation method with CH_4/O_2 mixture affected differently the activity and stability of the Ni/γ-Al_2O_3 and the Ni/α-Al_2O_3 catalyst. This activation method increased significantly the stability of Ni/α-Al_2O_3 compared to H_2 reduction. SEM and TG/DTA analysis indicate the formation of filamentous carbon during the CH_4/O_2 activation step, which is associated with the increasing catalyst activity and stability. The effect of temperature on the type of carbon formed was investigated; indicating that filamentous coke increased activity while encapsulating coke promoted deactivation. A discussion about carbon formation and the influence on the activity is presented.

Keywords: Ethanol steam reforming; Ni/Al2O3 catalysts; Deactivation, coke deposition

1. Introduction

In a few decades, the continuous rise of energy demand and the shortage of petroleum reserves may result in a critical situation, with exponential increase in energy cost. Hydrogen fuel cells are the most promising systems for energy production, since they are more efficient and environmentally clean than conventional thermal machines.

Natural gas is still the main source of hydrogen, due to its abundance. However, the development of alternative routes for hydrogen production employing renewable sources is of great interest due to economic and environmental reasons. In this context, ethanol steam reforming has attracted the attention of many researcher groups in the last years. It may become an important industrial process, especially for sugarcane producing countries. It is a cleaner process than methane steam reforming, because the CO_2 ''free'' cycle, which is generated in the reforming of ethanol and consumed by sugarcane photosynthesis.

Many studies have suggested Ni as the most suitable metal [1–4] for ethanol steam reforming. Although comparative studies [4–6] have shown better performance on basic supports, such as MgO and La_2O_3, alumina in γ or α phase is interesting due to its industrial use. The high surface area of γ-Al_2O_3 provides higher metal dispersion, while α-Al_2O_3 presents better mechanical resistance.

The coke deposition on Ni/Al_2O_3 catalysts is the main cause for deactivation during ethanol steam reforming [3,4]. The routes for carbon formation include Boudouard reaction, methane decomposition and polymerization of ethene, the latter originated from ethanol dehydration over Al_2O_3 acidic sites. Carbon deposition is thermodynamically unfavorable at high temperatures and higher water/ethanol ratios [7–9].

The direct deactivation of catalysts occurs predominantly by covering active phases, due to encapsulating carbon. Nevertheless, carbon may deposit over catalysts without deactivation [10], in a mechanism that includes: carbon deposition over metal surface, migration of carbon containing species to the

* Corresponding author.
E-mail address: schmal@peq.coppe.ufrj.br (M. Schmal).

0920-5861/$ – see front matter © 2007 Elsevier B.V. All rights reserved.
doi:10.1016/j.cattod.2007.01.062

bulk phase of metal, saturation of these species and condensation of carbon [11–13]. This mechanism results in the formation of filamentous carbon, which does not cause direct catalyst deactivation, but accumulates continuously, blocking the bed or breaking pellets.

It has been reported that the formation of filamentous carbon can result in a better catalyst activity performance. In another study by Schmal and co-workers [14], the method of reduction with hydrogen was compared with an activation method, using a mixture CH_4/O_2 in the ratio 2/1, for methane dry reforming. This method of activation resulted in filamentous carbon formation, which improved the catalytic performance for dry reforming.

To our knowledge, there is no study reporting the formation of different types of carbon, and its influence in ethanol steam reforming over Ni catalysts. The aim of this work is to study the deactivation of Ni/Al_2O_3 catalyst during ethanol steam reforming, and the influence of different forms of deposited carbon on catalyst activity and stability.

2. Experimental

2.1. Catalyst preparation

The catalysts were prepared by wet impregnation, using a $Ni(NO_3)_2{\cdot}6H_2O$ (Acros Organics) aqueous solution. After impregnation, catalysts were dried at 398 K during overnight and calcined by heating (10 K min^{-1}) in air (30 mL min^{-1}) to 823 K and holding for 3 h. Catalysts were prepared with 8 and 16% metallic loadings. NiO bulk was prepared from calcination of $Ni(NO_3)_2{\cdot}6H_2O$ at 773 K under air flow.

2.2. Catalyst characterization

The surface area and pore volume were obtained by nitrogen physisorption (Micromeritcs ASAP, model 2000). For temperature programmed reduction (TPR) analysis, catalysts (100 mg) were dried at 423 K for 1 h in Ar, followed by heating at 10 K min^{-1} from room temperature to 1273 K under 1.74% H_2/Ar mixture (30 mL min^{-1}). The quantity of hydrogen in the effluent was detected with a thermal conductivity detector (TCD). X-ray diffraction (XRD) was conducted using a Rigaku model Miniflex diffractometer (Cu Kα λ = 1.5418 Å). In addition, crystalline modifications during ethanol steam reforming reaction was investigated with *in situ* X-ray analysis, using a Rigaku D Max Ultima (Cu Kα λ = 1.5418 Å) equipped with Anton Paar XRK900 reduction chamber.

After activity testing, some catalysts were analyzed by to thermogravimetric analysis and differential thermal analysis (TGA/DTA) in a Rigaku TAS-100 apparatus. The catalysts were heated at 10 K min^{-1} under synthetic air flow, and the mass loss and temperature difference between the sample and the reference (α-Al_2O_3) were measured. SEM analysis of catalysts after activity tests were conducted in a JEOL JSM 6460LV apparatus, equipped with energy dispersive X-ray spectroscopy (EDS) (Thermo Noran System Six model 200), and the samples were coated with gold before analysis.

2.3. Activity tests

Catalysts (12 or 25 mg) loaded in a U shape quartz reactor were previously reduced in 16% H_2/He mixture (96 mL min^{-1}) at a heating rate of 10 K min^{-1} up to 973 K and held for 1 h at this condition. For the activation method, the same heating rate and temperature were employed with a flow of $He/CH_4/O_2$ mixture (47/22/11) at 80 mL min^{-1} [14]. After the reduction or activation procedure, catalysts were kept under helium flow for 30 min at 973 K, and cooled to ~373 K. The gas flow was switched to the reforming feed composition and adjusted to the reaction. The reactor was heated until reaction temperature without flow (around 20 min), and than switched to feed gas.

Ethanol and water were introduced using two separate saturators, kept at a controlled temperature, in order to obtain a constant molar fraction in the vapor phase. Helium supplied by mass flow controllers (MKS) was passed through both saturators. The reactor effluent was analyzed by gas chromatography (Varian CP 3800), equipped with a thermal conductivity detector (TCD) and flame ionization detector (FID). The effluent was analyzed with a Poraplot-Q column using He as the carrier gas.

For comparison between the hydrogen reduction and methane activation method, the following conditions were chosen for ethanol steam reforming. The volumetric flow rate through the catalyst (12 mg) was held at 200 mL min^{-1} with a composition of 0.05 atm ethanol, 0.15 atm water, and balance He (1 atm total pressure). The influence of temperature was examined in a flow rate of 100 mL min^{-1} with the same composition stated above using 25 mg of catalyst.

3. Results and discussion

3.1. Thermodynamic analysis

Thermodynamic analysis of carbon formation was done by minimization of Gibbs free energy as a function of temperature and various H_2O/EtOH ratios, as displayed in Fig. 1. According to the literature [7–9], the graphitic carbon formation is unfavorable at higher H_2O/EtOH ratios, as shown in Fig. 1, and is maximized around 773–873 K. This behavior suggests that the endothermic reaction of methane decomposition prevails at that temperature:

$$CH_4 \leftrightarrow C + 2H_2 \quad (\Delta H = 74\,kJ/mol)$$

The carbon gasification and Boudouard reaction may be also important routes for carbon deposition or removal, depending on conditions employed:

$$C + H_2O \leftrightarrow CO + H_2 \quad (\Delta H = 131\,kJ/mol)$$

$$C + CO_2 \leftrightarrow 2CO \quad (\Delta H = 171\,kJ/mol)$$

It can be observed that, for H_2O/EtOH ratios above 3, the graphitic carbon deposition is practically zero above 600 K.

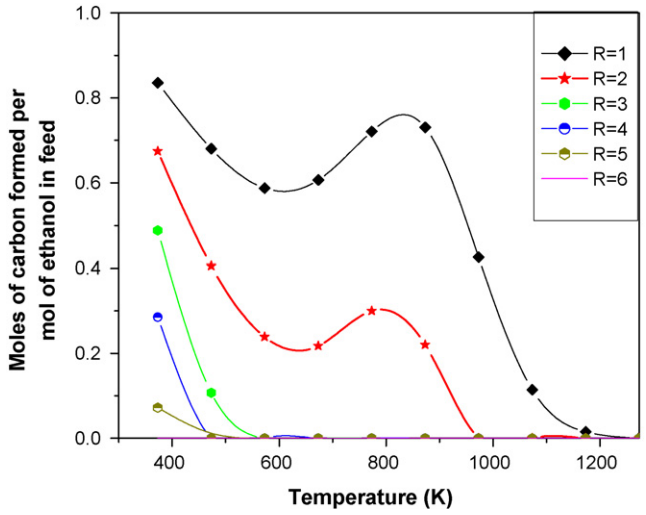

Fig. 1. Moles of carbon formed per mol of ethanol in feed for various R = H_2O/EtOH as function of temperature.

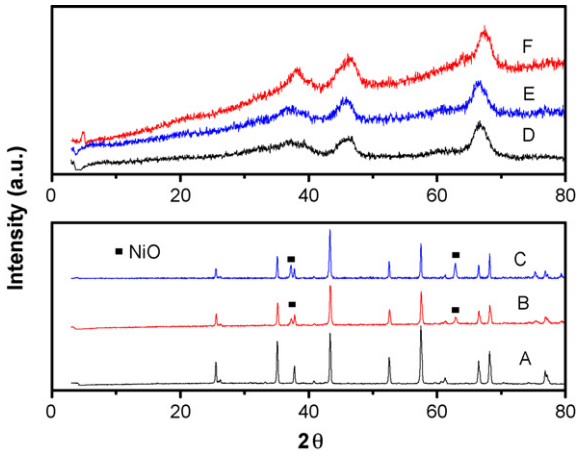

Fig. 2. XRD analysis of α-Al_2O_3 (A), 8% Ni/α-Al_2O_3 (B), 16% Ni/α-Al_2O_3 (C), γ-Al_2O_3 (D), 8% Ni/γ-Al_2O_3 (E), and 16% Ni/γ-Al_2O_3 (F).

3.2. Catalyst characterization

The surface area and pore volume are presented in Table 1. Results show that the surface area of α-Al_2O_3 is low, while γ-Al_2O_3 is high but decreases after impregnation with NiO, indicating blockage of pores. The final loading of NiO has little correlation with the loss of surface area.

3.2.1. X-ray diffraction (XRD)

The XRD results of the catalysts and supports are presented in Fig. 2. Diffractograms of the catalysts supported on α-Al_2O_3 display characteristic peaks for face centered cubic NiO, but the catalysts supported on γ-Al_2O_3 has no observable Bragg reflections due to NiO, which suggests the presence of very small NiO particles, or the formation of an amorphous surface nickel aluminate. According to Li and Chen [15], the diffusion of nickel ions during calcination into the alumina lattice sites is limited to the first few outer layers of the support, resulting in a material without three-dimensional long-range order.

3.2.2. Temperature programmed reduction (TPR)

The TPR results for NiO catalysts supported on α-Al_2O_3 and γ-Al_2O_3 are presented in Fig. 3. The reduction of bulk NiO starts only around 668 K [16], but is found to be highly dependent on the TPR conditions employed [17–20]. Fig. 3 has two H_2 consumption peaks for the α-Al_2O_3 supported catalysts. The low temperature peak is attributed to reduction of NiO with weaker interaction with the support, while at higher temperature peaks are associated with NiO incorporated into Al^{3+} ions,

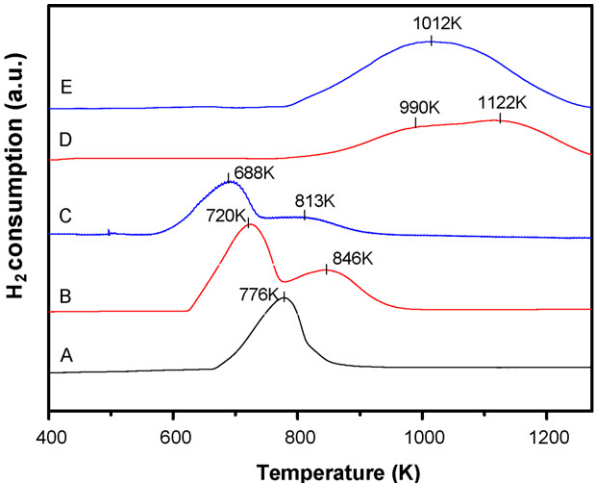

Fig. 3. TPR of NiO (A), 8% Ni/α-Al_2O_3 (B), 16% Ni/α-Al_2O_3 (C), 8% Ni/γ-Al_2O_3 (D), and 16% Ni/γ-Al_2O_3 (E).

originated from the support during the impregnation step [20,21]. Higher metal loading favors more easily reducible Ni species, as indicated by the lower temperature reduction peaks.

For the 16% Ni/γ-Al_2O_3 catalyst, peaks are not deconvoluted. However, the 8% Ni/γ-Al_2O_3 displays two different peaks, and a slight shift toward higher temperatures when compared to the 16% Ni/γ-Al_2O_3. The lower temperature peak is associated with small NiO particles with strong support interactions, while the higher temperature peak may be attributed to $NiAl_2O_4$ spinel phase [22,23].

Table 1
Textural properties of catalysts

	16% Ni/α-Al_2O_3	8% Ni/α-Al_2O_3	16Ni/γ-Al_2O_3	8% Ni/γ-Al_2O_3	γ-Al_2O_3	α-Al_2O_3
Surface area ($m^2\ g^{-1}$)	<10 [a]	<10 [a]	182	194	237	<10 [a]
Pore volume ($cm^3\ g^{-1}$)			0.57	0.78	1.03	

[a] Under detection limit.

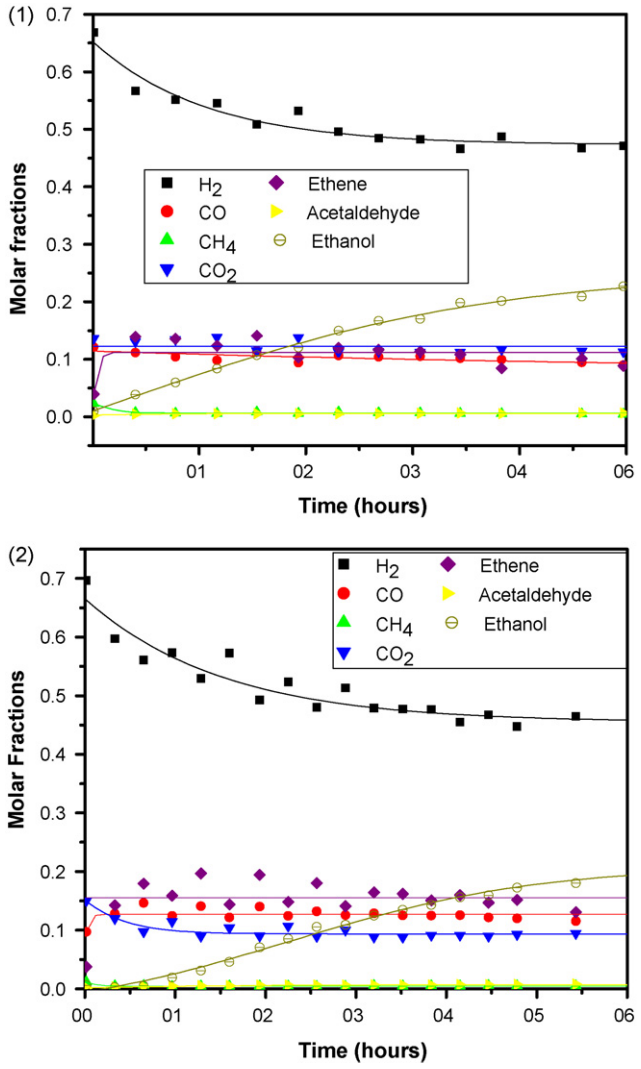

Fig. 4. Molar fraction for catalysts 16% (1) and 8% (2) of Ni supported on γ-Al_2O_3, except helium and water. Conditions: $\upsilon_0 = 200$ mL min^{-1}, $T = 873$ K, $m_{cat} = 12$ mg_{cat}, $P_{EtOH} = 0.05$, $P_{H_2O} = 0.15$, helium from balance.

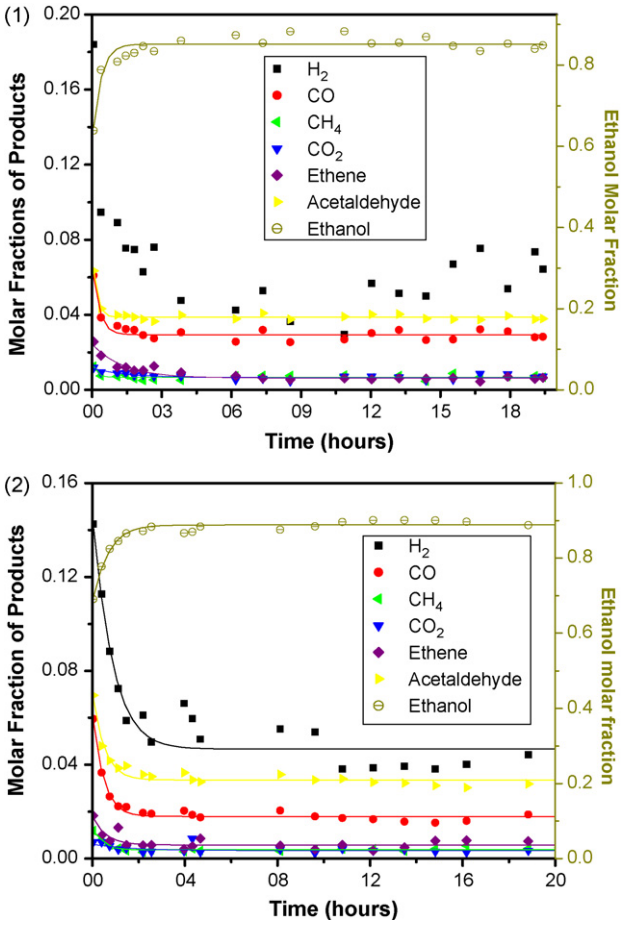

Fig. 5. Molar fraction for ethanol reforming over 16% (1) and 8% (2) Ni catalysts supported on α-Al_2O_3, except water and helium. Same conditions as in Fig. 4.

3.3. Activity tests

3.3.1. Effect of Ni loading

Fig. 4 shows the product distribution of ethanol reforming for Ni/γ-Al_2O_3 catalyst with different metal loadings. Under these conditions, both 8 and 16% Ni catalysts showed similar performance. The presence of ethene in the effluent indicates the influence of acidic sites on γ-Al_2O_3, which probably contribute to deactivation, according to the following reactions:

$$C_2H_5OH \leftrightarrow C_2H_4 + H_2O \quad (\Delta H = 45\,kJ/mol)$$

$$C_2H_4 \rightarrow \text{encapsulating\_coke}$$

Fig. 5 displays the product distribution of ethanol reforming on the Ni/α-Al_2O_3 catalyst, which showed a very low activity under the same conditions as presented in Fig. 4 for Ni/γ-Al_2O_3. As expected the dispersion of nickel on α-Al_2O_3 catalyst is lower than on γ-Al_2O_3 that was observed through CO adsorption by DRIFTS analysis (not shown). With increasing metal loading the activity was not significantly changed, not justifying higher amounts of metal. The observed initial deactivation can be related to Boudouard reaction or methane decomposition. The small amount of ethene formation suggests that its polymerization is not an important route for the catalyst deactivation.

3.3.2. Effect of an alternative activation process

Previous report [14] has shown that with an alternative activation process, using a CH_4/O_2 mixture and temperature programmed heating, the activity of the catalyst for dry methane reforming was high and with increased stability. The same activation process was used for both catalysts for ethanol steam reforming [14].

3.3.2.1. Ni/γ-Al_2O_3 catalyst. Fig. 6 shows the molar fraction of product distribution for 16% Ni/γ-Al_2O_3 catalyst. The formation of a large amount of ethene indicates that the main reaction occurring is ethanol dehydration over acidic sites on γ-Al_2O_3. The ethylene profile also suggests that its polymerization is the main route of catalyst deactivation due to the formation of encapsulating carbon.

TG/DTA analysis of the catalysts either reduced with H_2 or activated with CH_4/O_2 mixture, after ethanol steam reforming

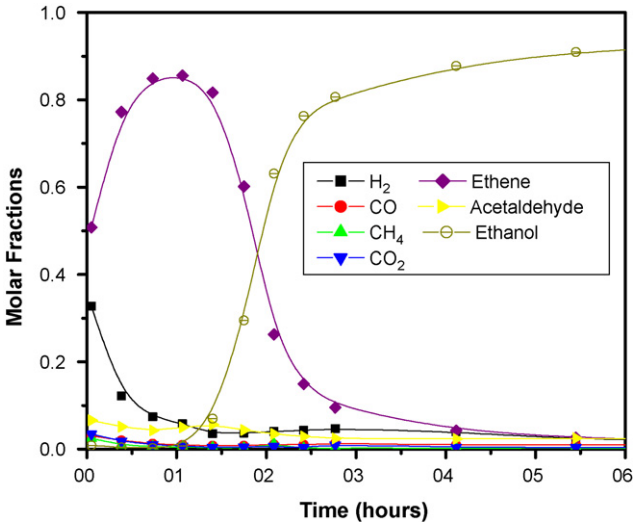

Fig. 6. Molar fraction of effluents for 16% Ni/γ-Al_2O_3 catalyst activated with the CH_4/O_2 mixture. Same conditions as in Fig. 4.

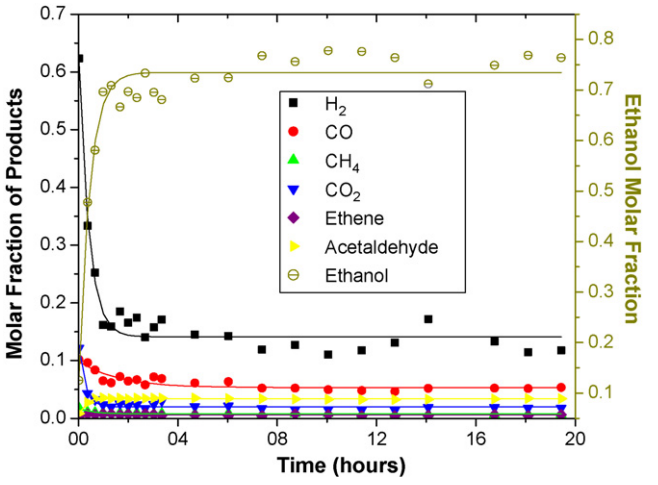

Fig. 8. Molar fraction for 8% Ni/α-Al_2O_3 catalyst activated with a CH_4/O_2 mixture, except helium and water. Same conditions as in Fig. 4.

are shown in Fig. 7. The TG results indicate the formation of a large amount of carbon deposited over the catalysts. DTA curves show the exothermic nature of carbon combustion. The origin of carbon species was observed through SEM analysis after reaction (not shown). SEM images did not show

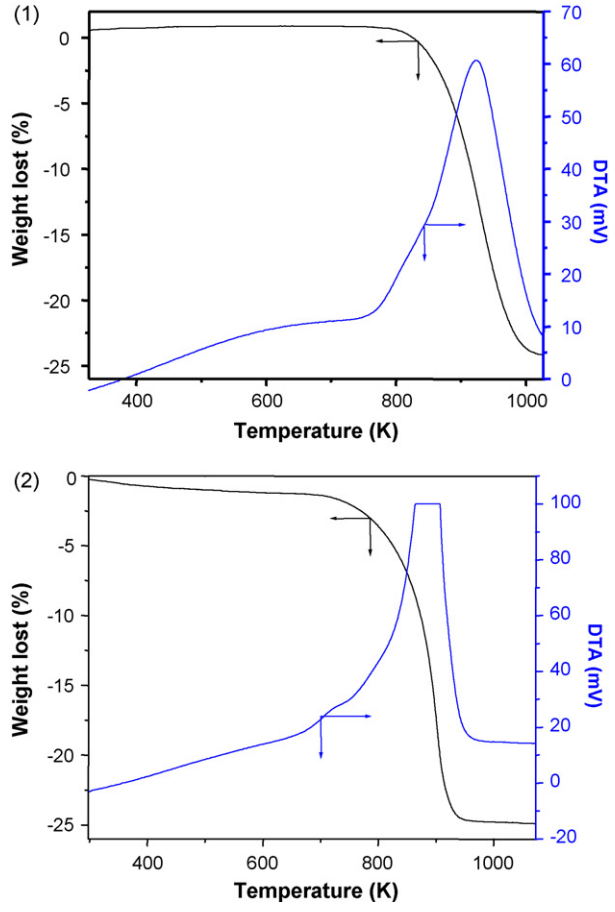

Fig. 7. TG/DTA analysis of Ni/γ-Al_2O_3: activated with a CH_4/O_2 mixture (1) and reduced with H_2 (2).

filamentous carbon, as expected [14], probably due to the strong interaction of Ni species with the support, as evidenced by TPR.

3.3.2.2. Ni/α-Al_2O_3 catalyst. Fig. 8 shows product distribution for the 8% Ni/α-Al_2O_3 catalyst for ethanol steam reforming after activation with CH_4/O_2. Comparing Fig. 8 and Fig. 5(2), there are significant differences in catalyst activity due to the activation method. Pretreating in the CH_4/O_2 mixture was better than reduction with pure H_2. It exhibits a very high initial activity, but does suffer significant deactivation. However, the conversion is still higher than the catalyst reduced with hydrogen. Both catalysts were analyzed by thermogravimetry after the reaction and results are shown in Fig. 9. The carbon deposited over the catalyst activated with a methane/oxygen mixture (∼20%) was greater than with H_2 (∼12%). The morphology after the reaction was analyzed by SEM (Fig. 10), and shows a large amount of filamentous carbon, as confirmed by EDS analysis (Fig. 11). These results agreed with previous one proposed by Souza et al. [14], indicating that small Ni particles are formed on filamentous carbon promoting a better performance, due to the migration of Ni at elevated temperature during the activation with methane/oxygen.

3.3.3. Effect of temperature on type of carbon formation

To investigate the nature of carbon formed during ethanol steam reforming on a 8% Ni/α-Al_2O_3 after reduction with H_2, the reforming of ethanol was examined at different temperatures. Fig. 12 shows the conversion of ethanol for different temperatures as a function of time. The initial conversion increased with temperature. For 773 and 873 K, the deactivation was very high, and the final conversions were lower than for 723 K after 20 min. On the contrary, for 973 K the deactivation was much lower and the final conversion was the highest.

In order to investigate structural changes during the reaction, *in situ* XRD analysis was carried out at 873 K. This temperature

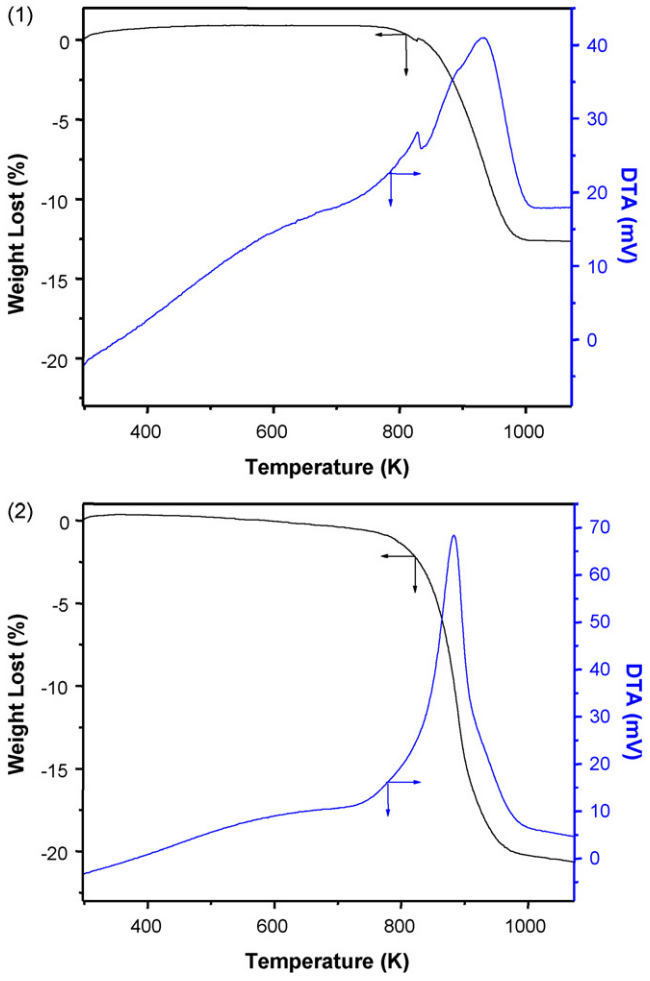

Fig. 9. TG/DTA analysis of Ni/α-Al_2O_3 catalyst: reduced with H_2 (1) and activated with a CH_4/O_2 mixture (2).

was chosen due the elevated deactivation and the results are shown in Fig. 13. It is important to stress that NiO was not observed in the diffractograms of reduced catalyst. The diffractograms remained unchanged during more than 20 h

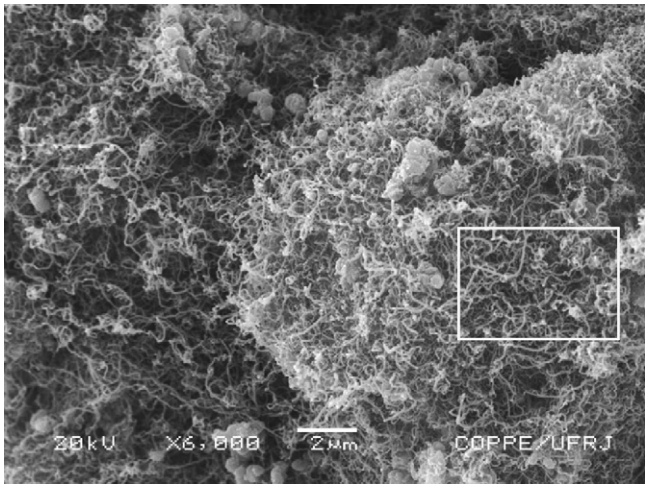

Fig. 10. SEM analysis of 8% Ni/α-Al_2O_3 catalyst activated with a CH_4/O_2 mixture after a reactivity test for ethanol steam reforming.

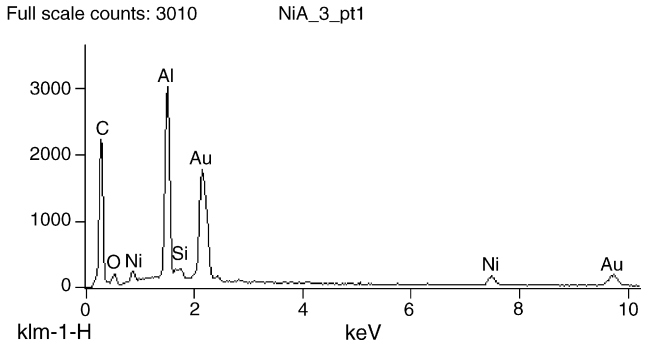

Fig. 11. EDS of marked region of Fig. 10.

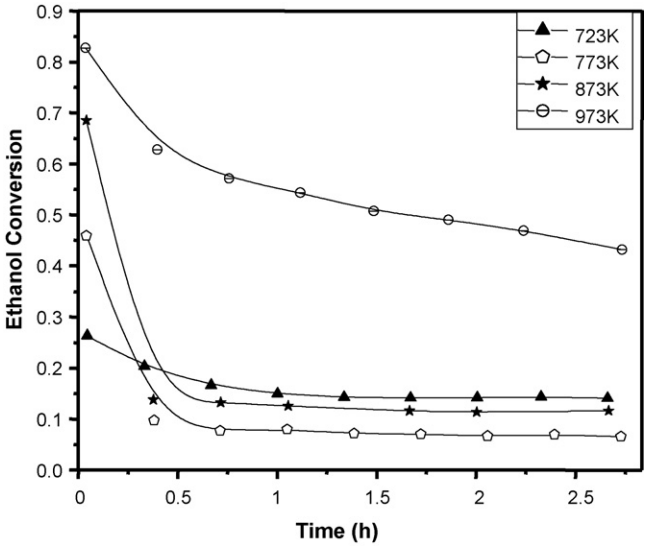

Fig. 12. Ethanol conversion on 8% Ni//α-Al_2O_3 for various temperatures as function of time.

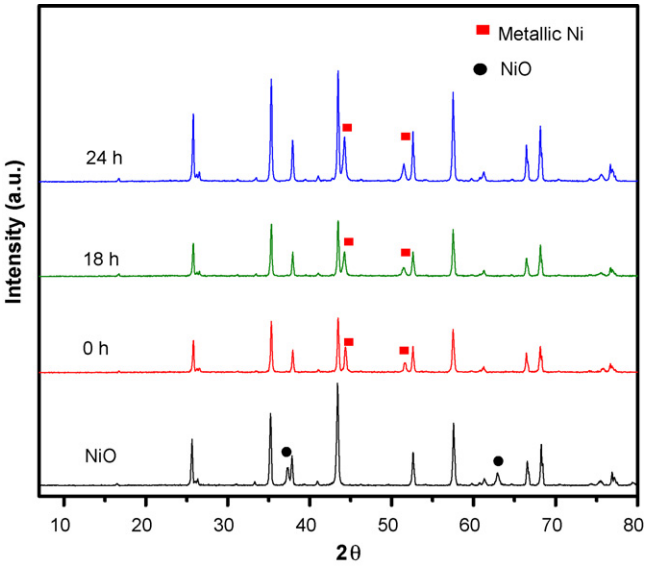

Fig. 13. *In situ* XRD analysis during ethanol steam reforming for catalyst 8% Ni/α-Al_2O_3 as function of time on stream.

of reaction. The XRD *in situ* measurements after different time exposure of reactants prove the presence of nickel particles and allow determining the dispersion of Ni during the reaction. The metallic dispersion, calculated using Scherrer equation, was constant over the whole experiment, and was less than 2%. Probably the main cause of deactivation is carbon deposition and not sintering. In fact, a great amount of carbon was deposited on the catalysts, as shown by TG analysis in Fig. 14.

The morphology of both catalysts with different procedure of deactivation, at 723 and 773 K, was investigated by SEM/EDS techniques, as shown in Fig. 15. The formation of graphitic carbon is thermodynamically unfavorable for all conditions, as demonstrated in Fig. 1, however, results demonstrate carbon formed in significant amounts. Deviations between thermodynamic predictions and experimental observations have been reported extensively in literature. Rostrup-Nielsen [24] explained that this behavior may be attributed to a structure disorder of carbon and a higher surface energy depending on the filament diameter. On the other hand, Manning et al. [25] and Bokx et al. [26] proposed the formation of an intermediate carbidic phase for such deviations, with different thermodynamic properties. These deviations may contribute to a minor carbon formation in equilibrium. Thermodynamic analysis cannot predict the formation of carbon inside the reactor, since the composition along the reactor is far from equilibrium. So, carbon formation is probably associated to kinetic restrictions, hindering carbon gasification, due to a competition between reactions generating and removing coke from catalyst [27].

The amount of filamentous carbon observed on this catalyst for the experiment carried out at 723 K was significant. In fact, TG analysis showed a weight loss around 45%. The high amount of carbon formation and the low decay of conversion of ethanol is a strong indication of prevailing formation of filamentous carbon, and not encapsulating carbon. The experiment carried out at 773 K showed the formation of filamentous carbon, however, in this case we observe fast deactivation, suggesting preferential formation of encapsulating carbon during the initial stages of the reaction. The same conclusion is suggested for the experiment at 873 K. The formation of encapsulating carbon results in the coverage of great number of metallic sites. Coke deposition is initially high and with time the rate of deposition decreases, because the majority of the metallic sites are becoming inactive.

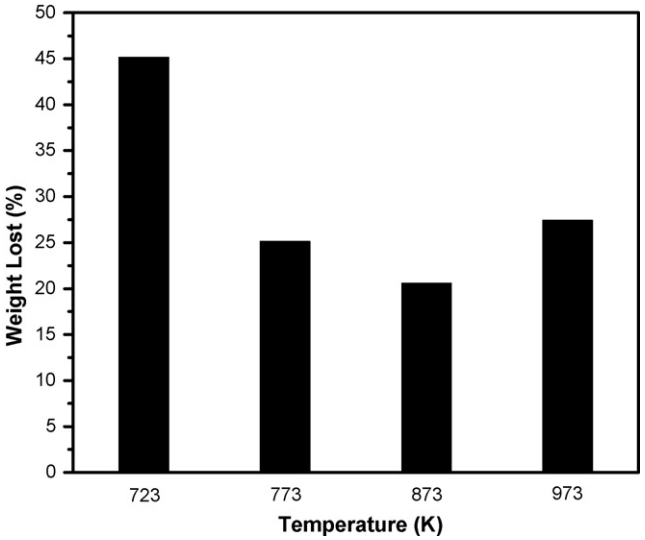

Fig. 14. Weight loss according TG/DTA analysis for the catalyst 8% Ni/α-Al_2O_3 at various temperatures.

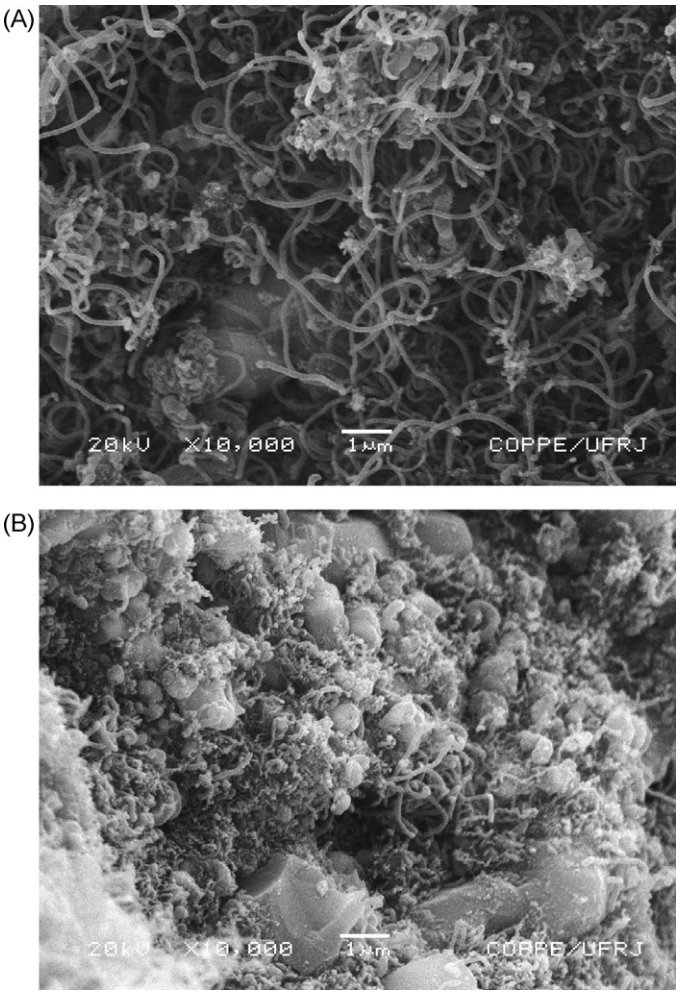

Fig. 15. SEM analysis of 8% Niα-Al_2O_3 catalyst after test at 723 K (A) and 773 K (B).

The experiment at 973 K demonstrated increasing carbon formation, as displayed in Fig. 14. However, it seems that the rate of carbon formation is quite similar as observed for 873 and 773 K. Probably, the low deactivation rate allows to a continuous carbon deposition and consequently more coke after 3 h of reaction. The results can be explained according to a hypothesis proposed by Rostrup-Nielsen and Trimm [28]. Carbon is deposited at the surface at a rate r_1; is gasified at a rate r_2; and reacts forming non-encapsulating carbon at a rate r_3, or encapsulating carbon at a rate r_4. The catalyst deactivation will occur when:

$$r_4 = r_1 - r_3 - r_2 > 0$$

At 723 K, the formation of filamentous carbon (r_3) seems to be practically equal the rate of carbon deposition (r_1). For the

range of 773–873 K, the rate of encapsulating carbon (r_4) becomes higher, leading to catalyst deactivation. Finally, at 973 K, the rate of encapsulating carbon decreases, maybe for higher carbon gasification (r_2) or lower carbon deposition (r_1).

4. Conclusions

The activity of Ni supported on γ-Al_2O_3 catalyst is higher than on supported α-Al_2O_3, because, according to XRD results, Ni particles are more dispersed compared to Ni crystallites on α-Al_2O_3. In addition, XRD *in situ* measurements after different time exposure of reactants prove the presence of nickel particles, allowing determining the dispersion of Ni during the ethanol reforming itself.

The higher surface area of γ-Al_2O_3 promotes the formation of ethene during ethanol steam reforming, which can lead to coke deposition. An alternative activation method with a CH_4/O_2 mixture rather than a standard hydrogen reduction activation step demonstrated that NiO on γ-Al_2O_3 was difficult to reduce, as evidenced by the product distribution during the steam reforming of ethanol, while on α-Al_2O_3, the activity was much higher, which can be attributed to the migration of Ni particles on carbon filaments.

Although the formation of graphitic carbon is not predicted thermodynamically under such conditions, coke deposition was observed and is probably associated to kinetic restrictions, hindering carbon gasification.

References

[1] F. Frusteri, S. Freni, V. Chiodo, L. Spadaro, G. Bonura, S. Cavallaro, Appl. Catal. A 270 (2004) 1.
[2] F. Auprête, C. Descorme, D. Duprez, Catal. Commun. 3 (2002) 263.
[3] S. Freni, S. Cavallaro, N. Mondello, L. Spadaro, F. Frusteri, Catal. Commun. 4 (2003) 259.
[4] A.N. Fatsikostas, D.I. Kondarides, X.E. Verykios, Catal. Today 75 (2002) 145.
[5] J. Sun, X.P. Qiu, F. Wu, W.T. Zhu, Int. J. Hydrogen Energy 30 (2005) 437.
[6] S. Freni, S. Cavallaro, N. Mondello, L. Spadaro, F. Frusteri, J. Power Sources 108 (2002) 53.
[7] K. Vasudeva, N. Mitra, P. Umasankar, S.C. Dhingra, Int. J. Hydrogen Energy 21 (1996) 13.
[8] E.Y. Garcia, M.A. Laborde, Int. J. Hydrogen Energy 16 (1991) 307.
[9] V. Mas, R. Kipreos, N. Amadeo, M. Laborde, Int. J. Hydrogen Energy 31 (2006) 21.
[10] E. Tracz, R. Scholz, T. Borowieki, Appl. Catal. 66 (1990) 133.
[11] H.S. Bengaard, J.K. Norskov, J. Sehested, B.S. Clausen, L.P. Nielsen, A.M. Molenbroek, J.R. Rostrup-Nielsen, J. Catal. 209 (2000) 365.
[12] Y.H. Mo, A.K.M.F. Kibria, K.S. Nahm, Synth. Met. 122 (2001) 433.
[13] J.R. Rostrup-Nielsen, J. Catal. 85 (1984) 31.
[14] M.M.V.M. Souza, L. Clave, V. Dubois, C.A.C. Perez, M. Schmal, Appl. Catal. A 272 (2004) 133.
[15] C. Li, Y.W. Chen, Thermochim. Acta 256 (1995) 457.
[16] J.A. Rodriguez, J.C. Hanson, A.I. Frenkel, H.Y. Kim, M. Perez, J. Am. Chem. Soc. 124 (2002) 346.
[17] J.T. Richardson, M. Lei, B. Thrk, K. Forester, M.V. Twigg, Appl. Catal. A 110 (1994) 217.
[18] Y. Li, B. Zhang, X. Xie, J. Liu, Y. Xu, W. Shen, J. Catal. 238 (2006) 412.
[19] H. Mori, C. Wen, J. Otomo, K. Eguchi, H. Takahashi, Appl. Catal. A 245 (2003) 79.
[20] D.C.R.M. Santos, J.S. Lisboa, F.B. Passos, F.B. Noronha, Braz. J. Chem. Eng. 21 (2004) 203.
[21] J.T. Richardson, M.V. Twigg, Appl. Catal. A 167 (1998) 57.
[22] S.C. Ho, T.C. Chou, Ind. Eng. Chem. Res. 34 (1995) 2279.
[23] J.L. Villacampa, C. Royo, E. Romeo, J.A. Montoya, P. Del Angel, A. Monzón, Appl. Catal. A 252 (2003) 363.
[24] J.R. Rostrup-Nielsen, J. Catal. 27 (1972) 343.
[25] M.P. Manning, J.E. Garmirian, R. Reid, Ind. Eng. Chem. Proc. Dev. Des. 21 (1982) 404.
[26] P.K. Bokx, A.J.H.M. Kock, E. Boellaard, W. Klop, W. Geus, J. Catal. 96 (1985) 454.
[27] J.M. Ginsburg, J. Piña, T.E. Solh, H.I. Lasa, Ind. Eng. Chem. Res. 44 (2005) 4846.
[28] J.R. Rostrup-Nielsen, D. Trimm, J. Catal. 48 (1977) 155.